"Babeş-Bolyai" University, Faculty of Physics, Cluj-Napoca, Romania
&
Interdisciplinary Research Institute on Bio-Nano-Sciences

LANTHANUM EFFECT ON TITANOSILICATE MICROSPHERES

PhD Thesis

Awatef Cheniti

Scientific coordinator:
Prof. dr. Simon Simion

Cluj-Napoca, 2012

TABLE OF CONTENT

Keywords: sol gel, spray dry, microspheres, titanosilicates, rare earth, thermal analysis, X-ray diffraction, Scanning electron microscopy, X-ray photoelectron spectroscopy, Electron paramagnetic resonance, Nuclear magnetic resonance, Raman and Infrared vibrational spectroscopies.

INTRODUCTION & MOTIVATION

The purpose of this thesis is to synthesise by spray-drying method oxide materials of scientific interest with interesting properties exploited in different applications. Following the successful development of numerous glasses containing rare earths, their potential applications in hot fields such as optical communications, lasers, sensors, but also in the biomaterials field, titanosilicate materials with lanthanum oxide have been synthesized and investigated by structural and morphological means.

Titanosilicate mixed oxides have attracted much attention, especially for catalysis and catalyst support materials, for the fact that silica-titania nanocomposites have higher photoactivity than pure TiO_2 [1,2]. The silica addition has also a significant influence on the surface properties of titanium dioxide, including the increase of the specific surface area of TiO_2 [3]. The addition of rare earths (RE) may change the physical and chemical properties of titanosilicate systems. In comparison with the pure TiO_2-SiO_2 samples, the RE-TiO_2-SiO_2 samples have relatively small particle size indicating that the doping with RE ions can improve the particle morphology, and delay the grain growth of TiO_2-SiO_2 during heat treatment, important phenomena in photocatalytic applications [4]. Thus, incorporation of lanthanide ions into a TiO_2 matrix provide La_2CO_5 phase formation on the surface and consequently enhance the photoactivity of titania [5-6]. Lanthanum oxide is used in optical glasses, to which this oxide confers low density, increased refractive index, hardness and chemical durability, since La_2O_3 has the largest band gap among the known rare earth oxides.

In a low concentration range of La_2O_3, these materials have a double functionality: as bio-materials and optical glasses. Not as extensive as in the field of photocatalysis [7-10], but there is a promising development also of titanosilicates in the field of biomaterials [11-15]. Titanium oxide and mixed silica-titanium oxide coatings prepared by sol gel process have already been applied in studies of cell adhesion, proliferation and response. It was found that the apatite grows better and also the cell attachment and proliferation increase on the surface of TiO_2-SiO_2 mixed oxide coating comparing to TiO_2 coating [16]. At the same time, it was reported that lanthanum enhances in vitro osteoblast differentiation but has no effect on type I collagen. Interestingly, lanthanum is rapidly emerging as a major player in the management of multiple other different systemic diseases especially in the field of oncology [17-21]. The

effect of rare earths addition on hydrophilicity of TiO_2/SiO_2 films was also reported, namely that the hydrophilicity of TiO_2 film is enhanced by both SiO_2 and La_2O_3 [22].

The thesis is divided in seven chapters, including the present introduction and conclusions. The second chapter deals with fundamental issues related to titanosilicate systems, the role of rare earth addition and their applications, describing also the defects in titanium and silica oxides. The third chapter describe the sol – gel method and spray dry process in order to obtain spherical particles with amorphous character and high homogeneity. The experimental methods are presented in the fourth chapter: thermal analysis, X-ray diffraction, scanning electron microscopy, X-ray photoelectron spectroscopy, Raman and Infrared spectroscopies, electron paramagnetic resonance and nuclear magnetic resonance spectroscopies. The fifth chapter present the setup devices used for sample synthesis.

The main part of this paper is the sixth chapter which describes the experimental results and comprises three parts. The proposal for the first part is the synthesis by spray-dry method titanosilicate microparticles with lanthanum oxide content in a low and high concentration range respectively. In this respect there were investigated in the last two parts the effects of both low and high lanthanum oxide content to the titanosilicate system and the thermal treatment influence on the physical and chemical properties that are of major interest in different applications mentioned earlier.

RESULTS & DISCUSSION

1. Synthesis by sol-gel and spray drying

Besed on the properties of titanosilicate systems with rare earth oxides and the advantages of the synthesis method presented in the theoretical part, TiO_2-SiO_2-La_2O_3-Gd_2O_3 materials were investigated. Therefore SiO_2:TiO_2=1:1 (atomic ratio) with xLa_2O_3 content (x = 0, 1, 5, 10, 15, 20, 50) samples doped with 1% Gd_2O_3 were prepared by using the spray method. Thus method, there was synthesized, at low-temperature and using a reduce number of unit operation, amorphous materials with high degree of homogeneity and purity. Since spray drying is a technique that can be easily automated and equipped for in-line product analysis. Not only the samples' properties, but also the production efficiency was improved.

Table 1. Sample' names, application fields, composition, calculated refractive index.

La_2O_3 concentration	Application fields	Name	Composition	Refractive index
Low La_2O_3 concentration range	Biomaterials Optical field Catalysis	TiSi	0%Gd_2O_3.100%(50%TiO_2+50%SiO_2+0%La_2O_3)	n=1.7300
		L0	1%Gd_2O_3.99%(50%TiO_2+50%SiO_2+0%La_2O_3)	n=1.7307
		L1	1%Gd_2O_3.99%(49.5%TiO_2+49.5%SiO_2+1%La_2O_3)	n=1.7390
		L5	1%Gd_2O_3.99%(47.5%TiO_2+47.5%SiO_2+5%La_2O_3)	n=1.7728
		L10	1%Gd_2O_3.99%(45%TiO_2+45%SiO_2+10%La_2O_3)	n=1.8138
High La_2O_3 concentration range	Optical field Catalysis	L15	1%Gd_2O_3.99%(42.5%TiO_2+42.5%SiO_2+15%La_2O_3)	n=1.8554
		L20	1%Gd_2O_3.99%(40%TiO_2+40%SiO_2+20%La_2O_3)	n=1.8970
		L50	1%Gd_2O_3.99%(25%TiO_2+25%SiO_2+50%La_2O_3)	n=2.1465

In the Figure 1 and Table 2 are presented the schematic representation of the syntheses process and the starting materials composition.

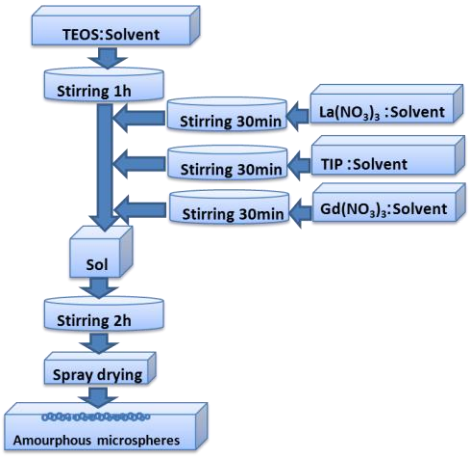

Figure 1. Stages for the preparation of TiO_2- SiO_2-La_2O_3 microspheres via sol-gel and spray-drying processes.

Table 2. The starting materials composition.

Starting materials		Ratio (weight%)
Precursors	Solvent	
TEOS	2-methoxyethanol	1 :2
TIP		1 :2
$Gd(NO_3)_3.5H_2O$		1 :10
$La(NO_3)_3.6H_2O$		1 :10

2. Nanostructured titanium silicates microspheres with low lanthanum content

$(50-x)\%TiO_2 \cdot (50-x)\%SiO_2 \cdot x\%La_2O_3$ (x = 0, 1, 5, 10) – further denoted as L0, L1, L5, L10.

2.1 Thermal analyses

Thermal properties of the as-prepared samples were studied by TGA-DTA analyses, used in order to distinguish the water loss, the organic component decomposition, the removal of nitrates, the beginning of the nucleation process and also the temperature of the maximum crystallization process and of the solid phase transition. The DTA curves were also used in order to establish the heat treatment temperatures required for obtaining amorphous samples without precursor's residues and polycrystalline oxide samples. Having in view the DTA data, the thermal treatment temperatures were settled at 350, 600, 700, 800, 900, 1000, 1100 and 1200°C. In the Figure 2 can be seen an example for L0 sample.

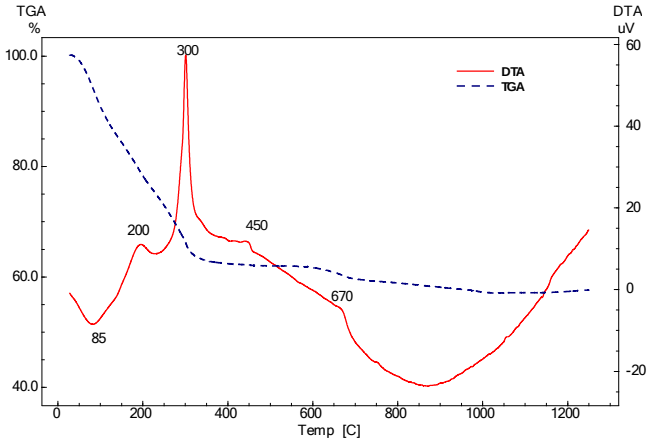

Figure 2. DTA and TGA curves for the L0 samples.

2.2 XRD

X-ray diffraction patterns of the as-prepared samples and of those heat treated at 350°C ones show an amorphous structure as revealed by the broad characteristic diffraction peak between $2\theta \sim 20°$ and 30° (Figure 3). This peak is slightly shifted for the heat treated microspheres above 350°C suggesting that another kind of arrangement exist inside of the amorphous state as a result of further dehydration and decarbonisation process that occurred after applying such thermal treatments. The L10 sample maintain the amorphous character up to 800°C, while the samples without and with less lanthanum content (L0, L1, L5) developed nanocrystals for the same annealing temperature and even for 700°C temperature (L0 and L1). At this temperature the X-ray patterns of these vitroceramics obtained after 30 minutes heat treatment at 700°C (Figures 3) show that in the glass matrix the crystalline phase identified as TiO_2 – anatase (21-1272) [23] was developed.

By increasing the heat treatment temperature, it is evidenced from the XRD patterns (Figure 3) that the first crystallization for the L0 and L1 samples is associated to anatase formation, while in the L5 sample first crystallise the rutile (21-1276). It seems that for L10

sample both anatase and rutile phases appear simultaneous at 900°C. By increasing the thermal treatment temperature one can observe that the amount of the rutile phase increases for the L0, L1 and L5 samples, while for L10 sample this crystalline phase decreases. An important aspect can be observed (Figure 3) for the L1 sample, where the anatase phase is present up to 1100°C, thus result will be confirmed by Raman analyses presented next (Figure 9).

A new phase $La_4Ti_9O_{24}$ (83-0946) can be identified after 1100°C heat treatment for L1 and at 1000°C for systems with higher lanthanum content (L5 and L10). Beside this dominant phase, La_2O_3 (22-0369) crystalline phase can be also observed at this temperature for the L5 and L10 systems. By increasing the thermal treatment temperature another two phases are developed: SiO_2 (coesite) (46-1045) and an unidentified lanthanum based crystalline phase. We can assume that this unidentified phase is based on lanthanum-titanium oxide ($La_xTi_yO_z$).

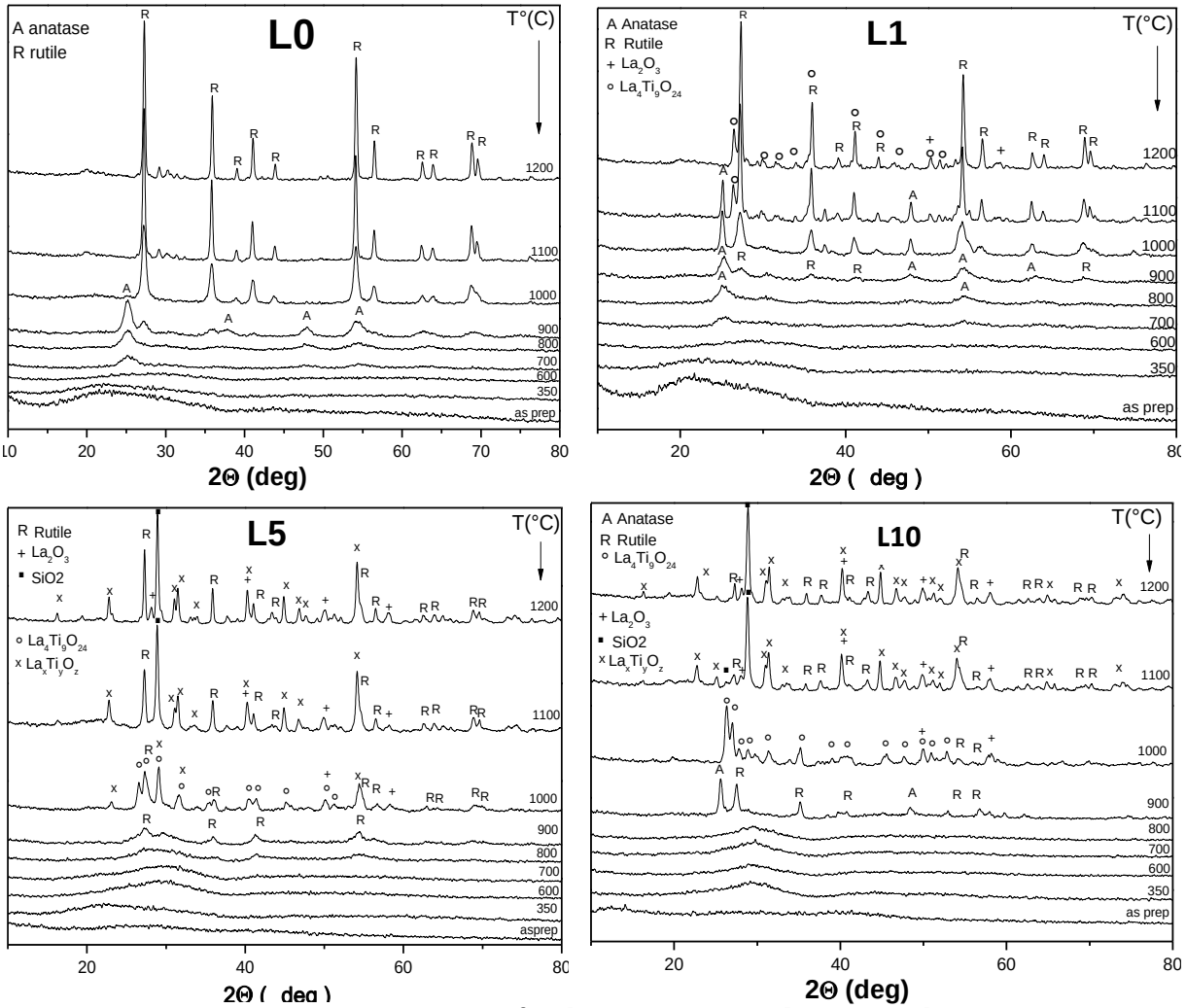

Figure 3. XRD patterns for the L0, L1, L5 and L10 samples.

2.3 SEM

The as-prepared samples were found to be microspheres as can be seen in (Figure 4). The SEM results show the obtained particles are very well defined and have a spherical shape with a diameter between 0.1 μm and 5 μm with a smooth surface without visible pores on the surface (Figure 4). For the samples 10% lanthanum content one can see that the microspheres walls have traces due to the collision with other microspheres in the spray cylinder. By increasing lanthanum content the microspheres walls are probably less rigid and can be distorted much easier. The traces have different sizes because the microspheres which produce them have different sizes.

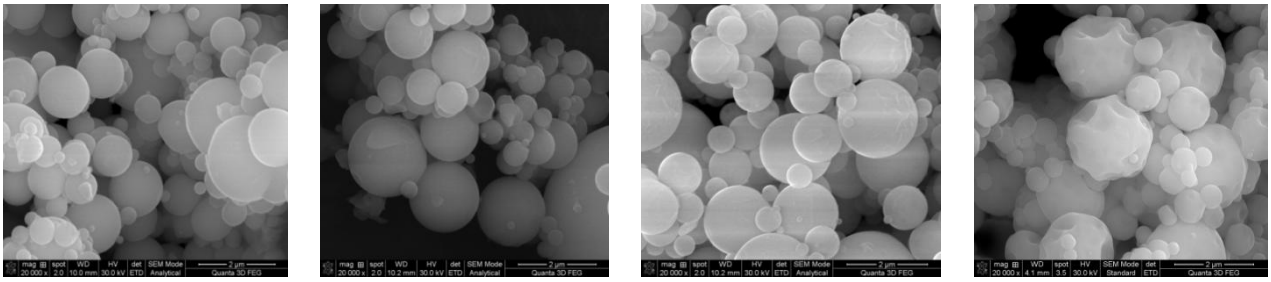

Figure 4. SEM images of the as-prepared L0, L1, L5 and L10 microspheres.

Scanning electron microscopy offers a better insight (Figure 5 and 6) regarding the coverage of titanium oxide nanocrystals by silica in amorphous state. In this respect it was used an ion beam cutting procedure performed by dual-beam FIB system in order to obtain cross-sectioned samples. By performing the cross-section it was proved that the microspheres are not hollow, like alumina-silicate microspheres reported for our group before [24].

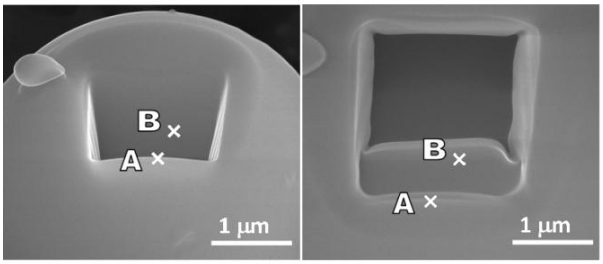

Figure 5. The SEM images (at different orientation) of the as prepared microspheres belonging to the L0 sample. Cross-section was performed by gallium ion beam cutting (A = edge, B = cross - section).

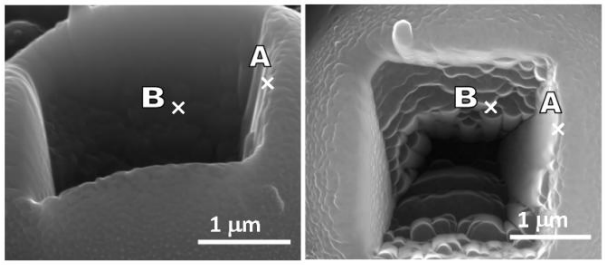

Figure 6. The SEM images (at different orientation) of the 1100°C thermally treated microspheres belonging to the L0 sample. Cross-section was performed by gallium ion beam cutting (A=edge, B=cross-section).

In the Figure 7 there are presented the SEM imagines for the 1100°C thermal treated samples belonging to the L0, L1, L5 and L10 samples at different magnifications. Can be observed the nanocristallites that are developed on the microspheres surface, according to XRD patterns.

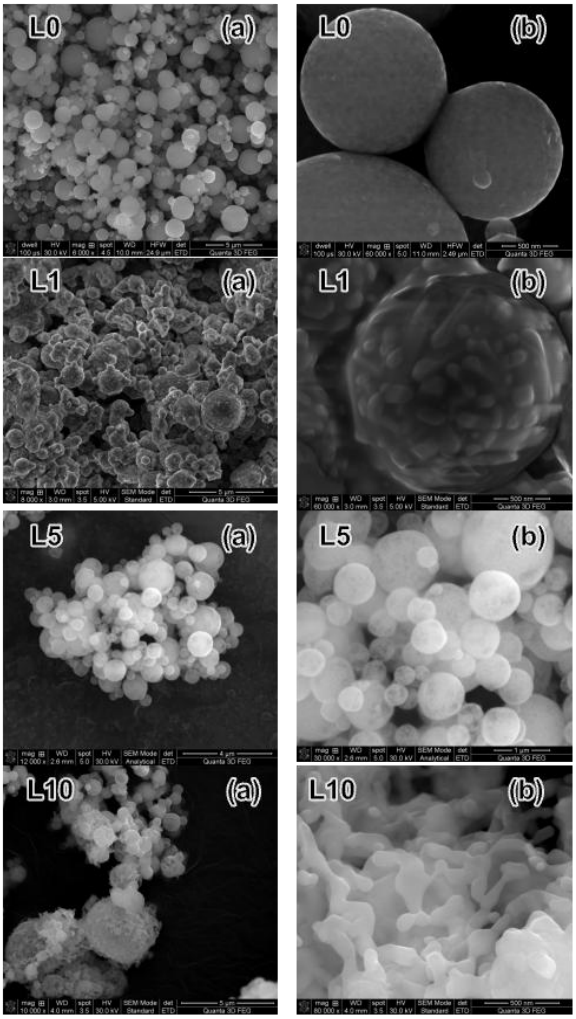

Figure 7. SEM imagines of the 1100°C heat treated L0, L1, L5 and L10 microspheres (a, b - different magnifications).

Table 3. The assignment of the selected infrared absorption bands of the as-prepared and heat treated samples.

Wavenumber (cm^{-1})	Band assignments
1650	HOH
1597	C=C
1509, 1406, 1382	C-O, CO_2
1046	CH_3
939	C-C
1080, 950	Ti-O-Si
800-650	Ti-O-Ti (Rutile)
640, 525, 470, 410	La-O, La_2O_3
884, 845, 532, 476	Si-O-Si

2.4 FTIR

The recorded FTIR spectra fot L0 and L10 samples are presented in the Figure 8 and and the infrared absorption bands assignments in Table 3.

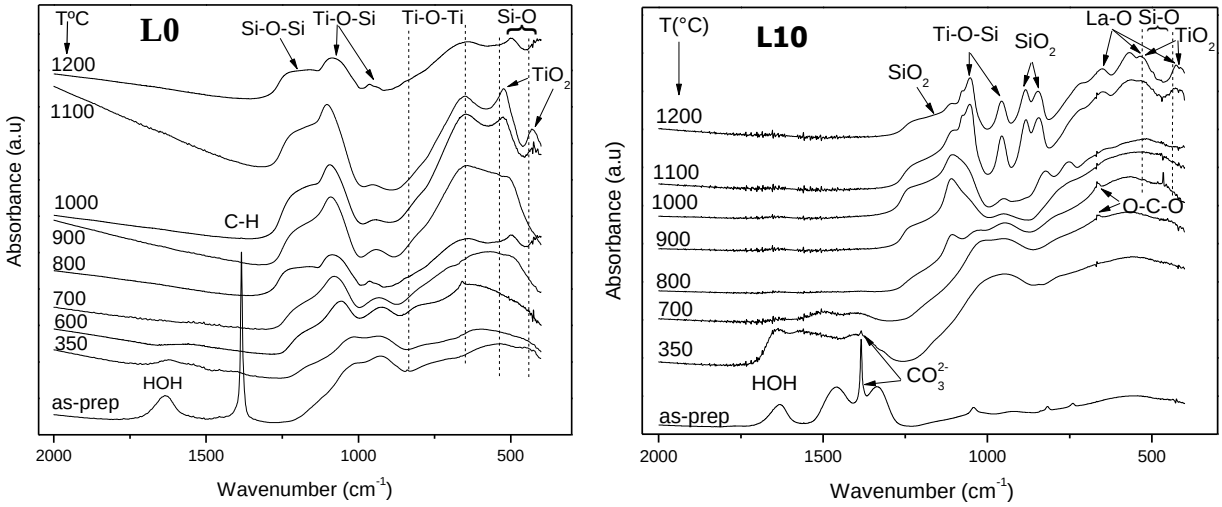

Figure 8. FTIR spectra of the L0 and L10 samples.

2.5 Raman

There is no interpretable signal in the Raman spectra of the samples annealed at 350, 600, 700 and 800°C thermal treated samples due to the fluorescence phenomena. In the (Figure 10) one can see only the D and G carbon vibration bands specific that overlaps with the fluorescence one.

For the **L1** sample (Figure 9), the bands at 150, 400, 525 and 645 cm^{-1} can be associated with the anatase phase that is clearly observed in the case of the sample heat treated at 900°C. By increasing the thermal treatment temperature the peaks intensity increases and we can see also the anatase peaks until 1100°C, which result was shown by XRD patterns. These Raman peaks disappear from the spectrum of the sample annealed at 1200°C. The presence of the anatase phase until such a high temperature (1100°C) is the highlight of this research.

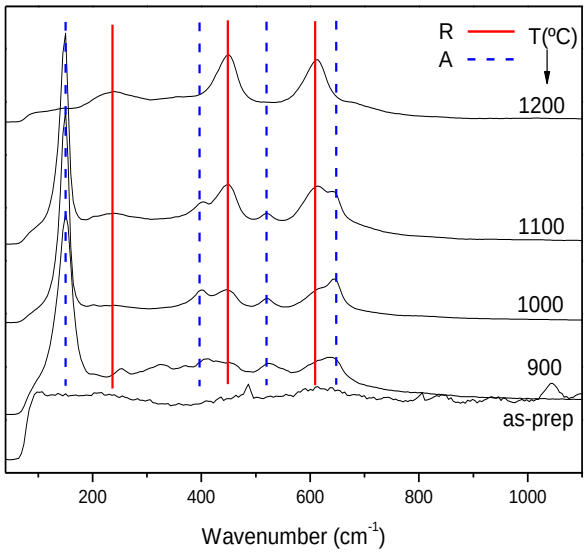

Figure 9. Raman spectra of the L1 samples.

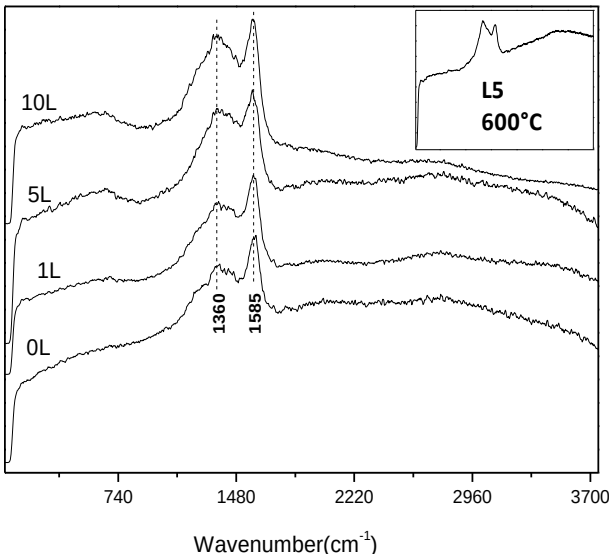

Figure 10. Raman spectra of the L0, L1, L5 and L10 microspheres, 350°C thermal treated. The insert specum represent an example for 600°C heta treatment – L5.

2.6 EPR

The gadolinium doping allowed using Gd^{3+} ions as paramagnetic resonance centres sensitive to their surrounding and able to inform on the structural changes occurred in their vicinity due to changes in the matrix composition and in the crystallinity degree [25-28]. When Gd^{3+} ions are introduced in low concentrations in glass matrices, they usually exhibit three typical signals with effective g-values of $g \approx 5.9$, 2.8 and 2.0, due to Gd^{3+} ions located at sites with intermediate and weak crystal fields respectively, a characteristic of so called U-spectrum of Gd^{3+} ions in disordered matrices [25,26,29,30]. All the spectra are dominated by

a large line centered at g ≈ 2.0, that reflects a relaxed and desordered vecinity in the amorphous matrices, but small features at g ≈ 5.9 and 2.8 are also observed. This indicates that there are sites in the non-crystalline matrices where the Gd^{3+} ions are experiencing intermediate field. The linewidth at g ≈ 2.0 of the EPR spectra, which directly reflects the changes in the spin-lattice relaxation rate and most importantly the structural disoder arround Gd^{3+} ions, changes by heat treatment at higher temperature.

The structural changes induced in amorphous titanium-silicates samples by heat treatment are well reflected in the EPR spectra of partially crystalline samples (Figures 11). The large line with g ≈ 2.0 in all heat treated microspheres shows that Gd^{3+} ions are preponderantely disposed in the residual non-crystalline phase, experiencing weak crystal fields, resulting from structural relaxation, but with still a high degree of disorder arround them. The EPR spectra indicate that the thermal annealing process plays a significant role in the formation of additionally paramagnetic centres.

For the as-prepared microspheres the EPR signal comes only from Gd^{3+} ions. For the L0, L1 and L5 heat treated microspheres the peak around g~2.004 can be attributed to oxygen vacancies [31]. For the L10 system this signal is not present and can conclude that the lanthanum addition inhibits the oxigen vacancies formation.

Similar EPR signal with the one arround g~2.004 has been observed in C-doped anatase [32], B-doped TiO_2 [33] or N-doped TiO_2 [34]. It was [35] also assigned in the literature the signal at g = 2.003 – 2.005 to the one electron trapped on the oxygen vacancy.

For the microspheres with lanthanum content new phases containing lanthanum are developing at this high thermal treatment according with XRD patterns (Figures 3). EPR spectra evidence the Gd^{3+} integration in these phases. The EPR spectra at high heat treatments are complicate to be resolve because of the multitude of phases developed at this temperature. For the 1100 and 1200°C the Gd^{3+} ions are probably integrated in the unidentified phase for the both L5 and L10 systems (Figure 11).

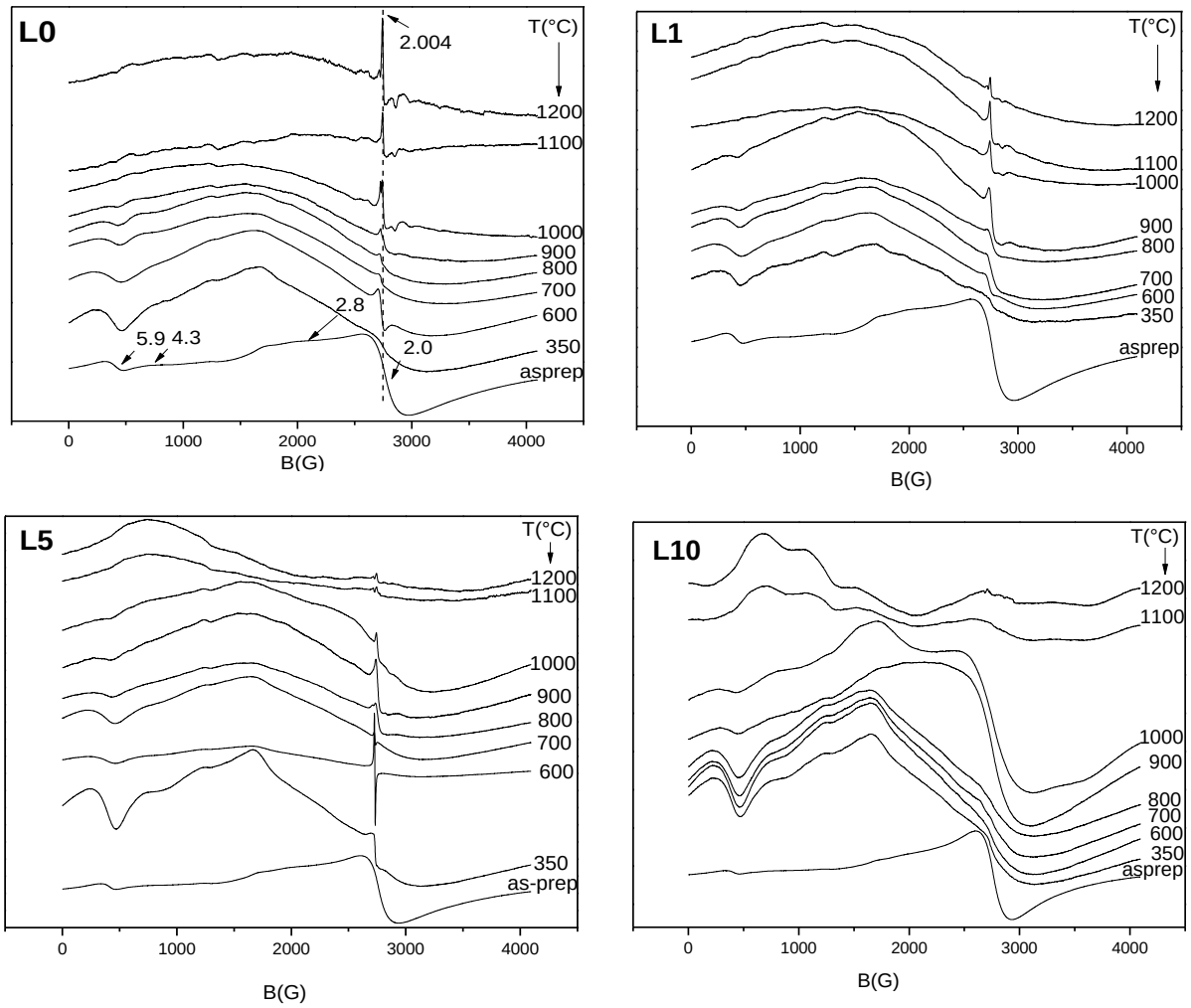

Figure 11. EPR spectra of the as-prepared and annealed L0, L1, L5 and L10 samples.

2.7 NMR

Structural MAS-NMR analysis was carried out on ^{29}Si nuclei, considering the four coordinated state of silicon in SiO_4 tetrahedra linked to form the silicate glass network. According to $Q^{(n)}$ notation, where $n \leq 4$ represents the number of bridging oxygen, the values of the chemical shifts denote the presence of certain silicate units/species [36].

The distribution of silicate tetrahedra can be estimated from ^{29}Si MAS- NMR spectra by deconvolution with components having chemical shifts corresponding to different $Q^{(n)}$ units. The ^{29}Si MAS- NMR spectra deconvolution was realized with DmFit program [37].

The ^{29}Si MAS NMR spectra of the L0, L1, L5 and L10 as-prepared sample (Figure 12) indicate the presence of Q^4, Q^3, Q^2, Q^1 and Q^0 units. The deconvolution procedure performed for all samples (illustrated an example in Figure 13 for L5 as-prepared sample) led to the results summarized in Table 4.

From the chemical shift of the Q^n units (Table 4 and Figure 12) can be observed a slight shift to higher ppm values, result that indicates that some changes of the SiO_2 units took place in the amorphous matrix, by increasing the lanthanum content. The relative fraction of the Q^n units and the width of the corresponding lines were calculated (Table 4) and represented in the Figure 12 for the as-prepared L0, L1, L5 and L10 samples. From these data can be concluded that the L0 sample shows the highest degree of disorder (compared with L1, L5 and L10 samples), while the L1 sample shows the lowest one.

From the NMR results we can conclude that SiO_2 segregation took place, by increasing the lanthanum content.

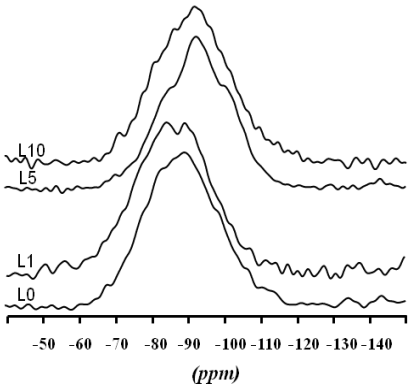

Figure 12. ^{29}Si NMR spectra of the L0, L1, L5 and L10 as-prepared samples.

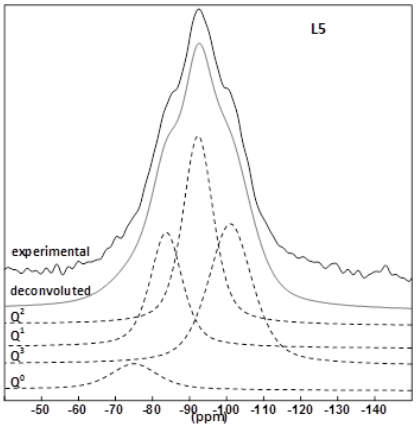

Figure 13. ^{29}Si NMR deconvolution of the experimental spectrum of the as-prepared L5 sample.

Table 4. Isotropic ^{29}Si chemical shift (A), relative fraction (%) (B) and width (C) of Q^n units data for the as-prepared L0, L1, L5 and L10 microspheres.

Q^n (ppm) / X (% La)	Q^0	Q^1	Q^2	Q^3	Q^4
0	-75	-81.28	-89.99	-101	-
1	-70.82	-82.05	-91.12	-99.64	-
5	-75	-83.7	-92.3	-101	-
10	-72.93	-82.1	-92.6	-	-109.13

Q^n (%) / X (% La)	Q^0	Q^1	Q^2	Q^3	Q^4
0	6.98	10.11	61.9	21	-
1	14.51	36.32	31.22	17.95	-
5	7.04	21.91	34.06	36.7	-
10	6.81	9.89	71.13	-	12.16

Q^n (ppm) / X (% La)	Q^0	Q^1	Q^2	Q^3	Q^4
0	-75	-81.28	-89.99	-101	-
1	-70.82	-82.05	-91.12	-99.64	-
5	-75	-83.7	-92.3	-101	-
10	-72.93	-82.1	-92.6	-	-109.13

2.8 XPS

XPS survey spectra showed the presence of C, O, Si, Ti and La as it was expected (Figures 14 and 15). Upon further analysis performed by using high resolution, XPS core level spectra were obtained for Si 2p (110-90eV), Ti 2p (470-450eV), La 3d (870-820eV), O 1s (545-520eV) and C 1s (295-270eV), presented and detailed in the thesis. Carbon adsorption usually takes place on all surfaces exposed to the atmosphere and is detected by the XPS technique, but it can also originate from the organic molecule, which are not completely removed from the nanoparticles surface and to the adsorbed carbon dioxide [38].

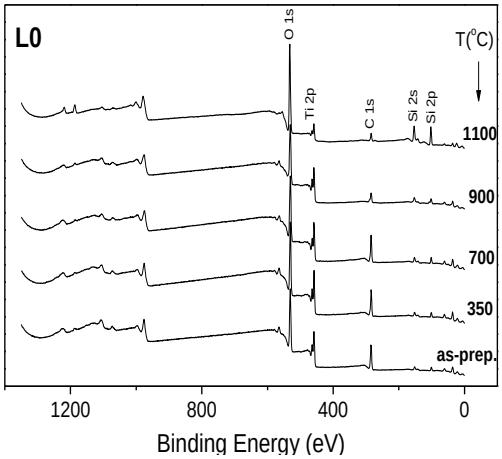

Figure 14. XPS survey spectra of the L0 microspheres.

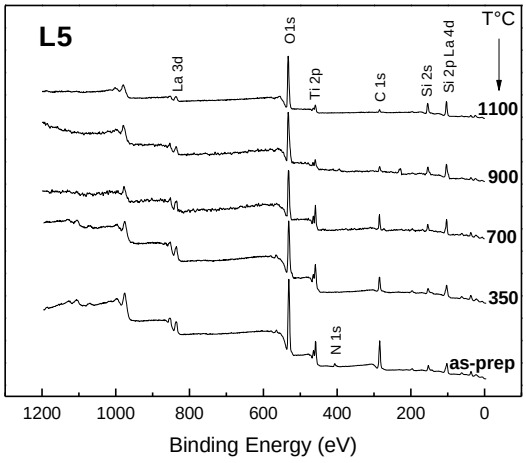

Figure 15. XPS survey spectra of the L5 microspheres.

From Tables 5 can be observed that the carbon concentration on the surface deacreases by increasing the heat treatment temperature as a result of the organic compounds removement. The relative percentage of the main components before and after heat treatment determined from the survey spectra of both systems reveals that the amount of Ti 2p at the surface decreases by appling the thermal treatment, while the percentage of Si 2p at the surface increases, concluding that the microspheres surface is covered by a silica layer.

Table 5. Relative percentage of the main components before and after heat treatment determined from the survey spectra of the L0 and L5 microspheres.

T(°C)	Elemental composition (at.%) – L0				Ti/Si
	O	C	Ti	Si	
as-prepared	50.2	30.3	9.3	10.2	0.91
350 °C	50.1	21.7	10.9	17.3	0.63
700 °C	50.1	19.6	10.2	20.1	0.5
900 °C	49	22.3	7.5	21.2	0.35
1100 °C	52.4	8.4	2.3	36.9	0.06

T(°C)	Elemental composition (at.%) – L5					Ti/Si
	O	C	La	Ti	Si	
as-prepared	43	42.6	1.3	5.7	7.4	0.77
350 °C	49	32.3	1.7	8.5	8.5	1
700 °C	51.4	27.6	1.6	8.4	11	0.76
900 °C	70.2	13.2	1.4	3.4	11.8	0.28
1100 °C	62.2	7.8	0.9	3.4	25.7	0.13

3. Nanostructured titanium silicates microparticles with high lanthanium content

$(50-x)\%TiO_2 \cdot (50-x)SiO_2 \cdot xLa_2O_3$ (x = 15, 20, 50) - further denoted as *L15, L20 and L50*

3.1 XRD

The XRD patterns of the L15, L20 and L50 samples show (Figures 16) different crystalline phases. In the 350-600°C temperature range only the La_2CO_5 (23-0320) phase is evidenced for all L15 and L20 samples. The diffraction pattern for L50 sample shows that the microparticles are mainly amorphous but some reflections due to the nucleation process of La_2CO_5 crystalline phase occur beginning from 650°C.

By increasing the calcination temperature, the decomposition of this phase took place, according with DTA data and La_2O_3 (05-0602) crystalline phase developed:

$$La_2O_2CO_3 \rightarrow La_2O_3 + CO_2$$

The transition temperature from La_2CO_5 to La_2O_3 crystalline phase increases by increasing the lanthanum oxide.

Because of the shape of the XRD pattern at 700°C for the L50 sample it was difficult to identify the phases that are developing at this temperature. Therefore there were performed two additional heat treatments at 650 and 730°C. If the La_2CO_5 to La_2O_3 transition was completed at 700°C for the first two systems (L15 and L20), the XRD patterns for the third one (L50) evidenced that the both phases coexist (La_2CO_5 and La_2O_3) at this temperature and the transition is completed only at 730°C. After (Figure 16) the calcinations at 700°C, mixtures of several lanthanum oxycarbonates were obtained for L50 sample, in good agreement with the literature [39].

The La_2O_3 phase is developing from 700°C for the L15 and L20 samples and can be observed until 1000°C and 1200°C termal treatments, respectively.

Above 700°C calcinations temperature, nearby the La_2O_3 crystalline phase resulted by La_2CO_5 decomposition, a small amount of TiO_2-rutile phase is developing for L15 sample and can be identified up to 1200°C. This phase can be evidenced for L20 sample in the 800°C - 1200°C temperature range. Should be noted that the rutile phase is not developing at any thermal treatment for the microparticled with highest lanthanum content (L50).

By increasing the thermal treatment at 1000°C the $La_2Ti_2O_7$ phase is developed for L15 and L20 samples. Beside $La_2Ti_2O_7$ phase, SiO_2 (coesite) phase and small amounts of other crystalline phase are developed. At 1100°C and 1200°C the $La_2Ti_2O_7$ crystalline phase cannot be observed and the $La_xTi_yO_z$ phase developed at 1000°C become predominant nearby the coesite phase.

The XRD patterns for the L50 system heat treated from 800 up to 1200°C show the development of three phases: $La_{9.33}Si_6O_{26}$ apatite phase (49-0443), La_2TiO_5 (15-0335) and SiO_2 (coesite). One can observed that the developing temperatures for apatite phase, SiO_2 and La_2TiO_5 are 800°C, 900°C and 1000°C, respectively. All these three phases can be identified in XRD patterns for the 1100°C thermal treated microparticles. The increase of the calcination temperature leads to the increase of the intensity peaks of these phases.

The crystallization temperature of this apatite phase is quite low compared to single-phase $La_{9.33}Si_6O_{26}$ prepared by a solid-state reaction (1500°C) [40,41].

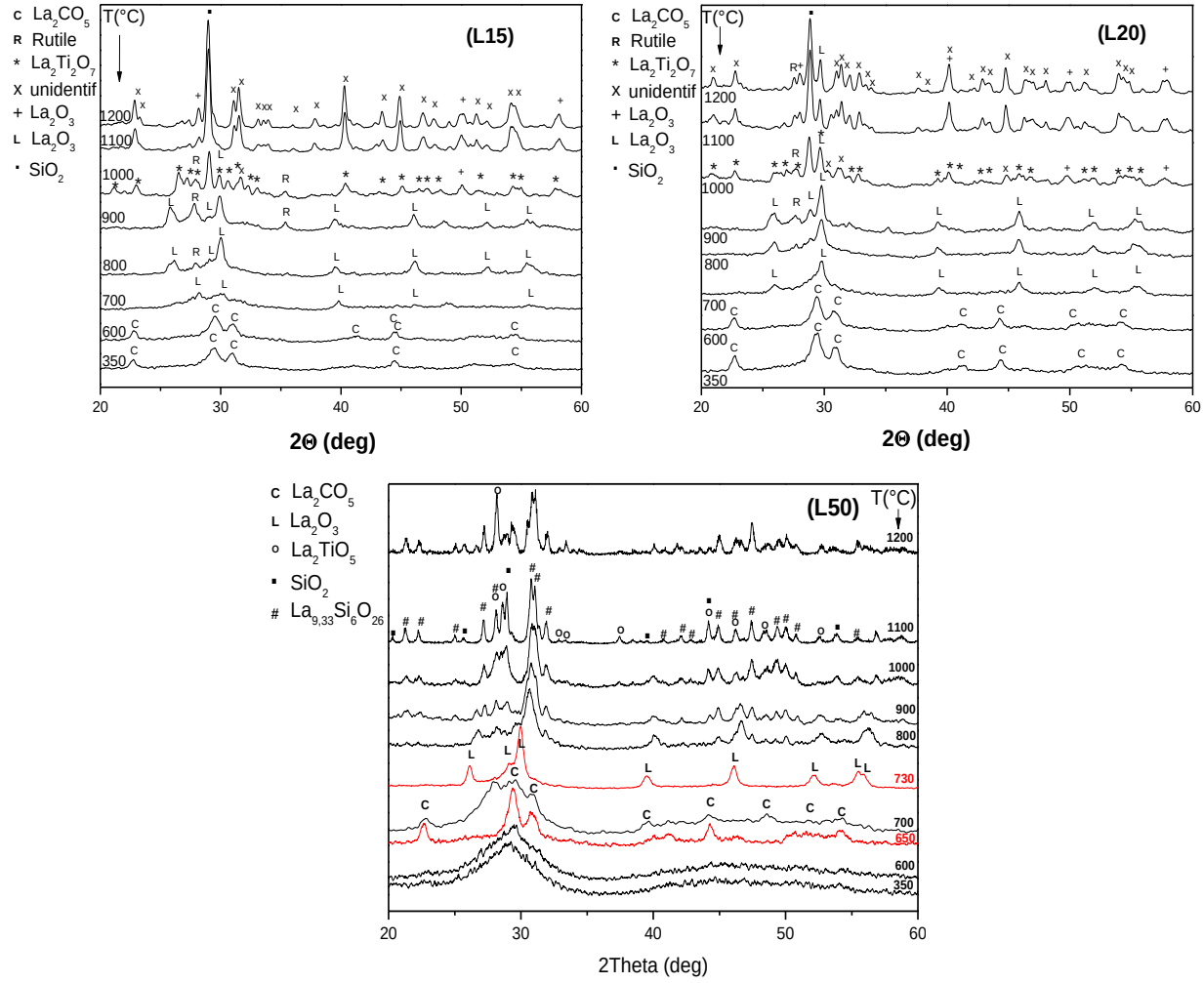

Figure 16. XRD patterns of the L15, L20 and L50 samples.

3.2 SEM

In the SEM images for the as prepared samples (Figure 17) one can see that only in the case of L15 were obtained microspheres. The L15 microspheres' walls have more traces due to the collision with other microspheres in the spray cylinder than the L10 ones presented before. By increasing the thermal treatment cannot be observed a spherical shape, but an enhanced microparticles agglomeration (Figure 18). The spray dried samples with higher lanthanum content consists in microparticles as can be observed in Figure 18.

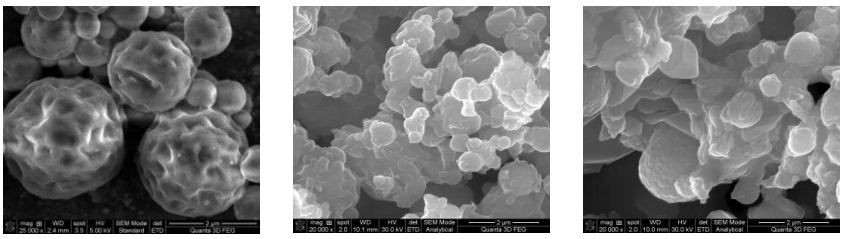

Figure 17. SEM imagines of the as-prepared L15, L20 and L50 microparticles.

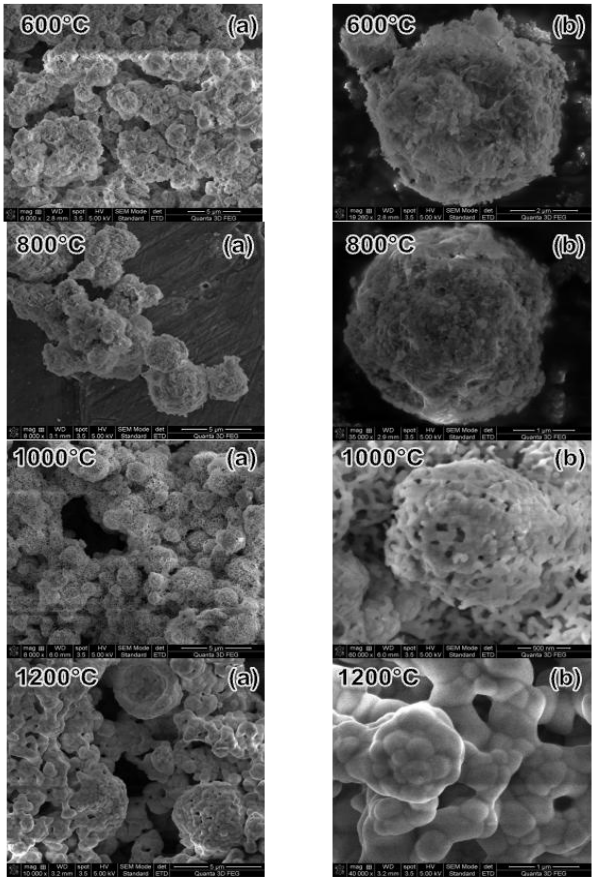

Figure 18. SEM imagines for L15 sample at different thermal treatments and magnifications (a, b).

By increasing the heat treatment for the highest lanthanum concentration sample (L50) the particle size occur diminished due to both removal of water and organic molecules still resident in the spray dried samples and to densification and structural changes [42]. The diminished microparticles lead to the formation of high porosity degree agglomerations.

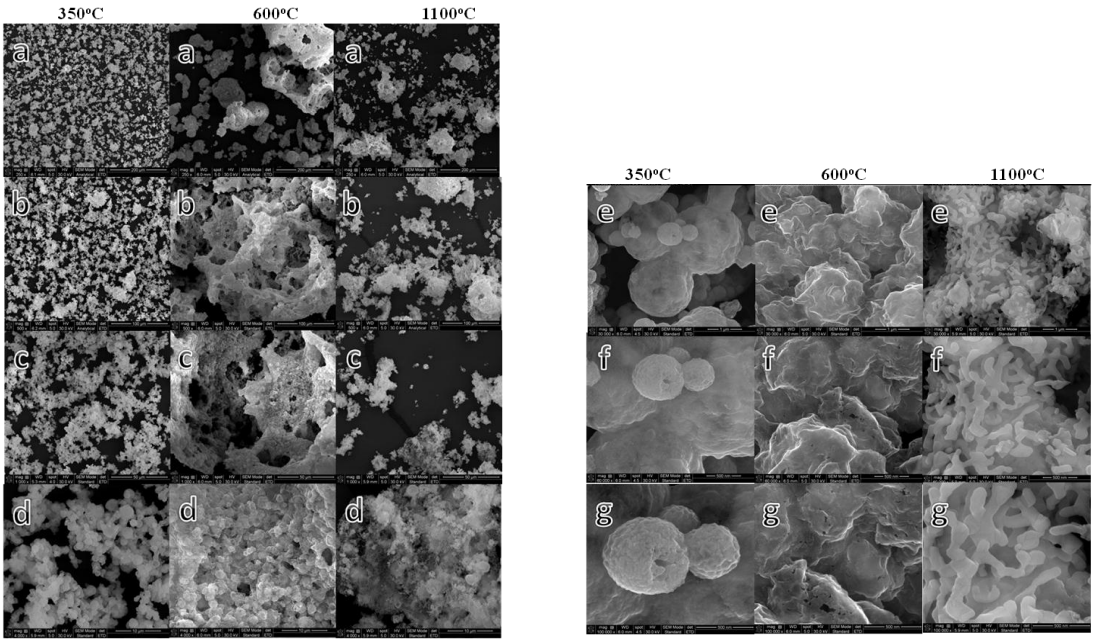

Figure 19. SEM images of the L50 microparticles at different thermal treatments and magnifications (a, b, c, d, e, f , g).

3.3 FTIR

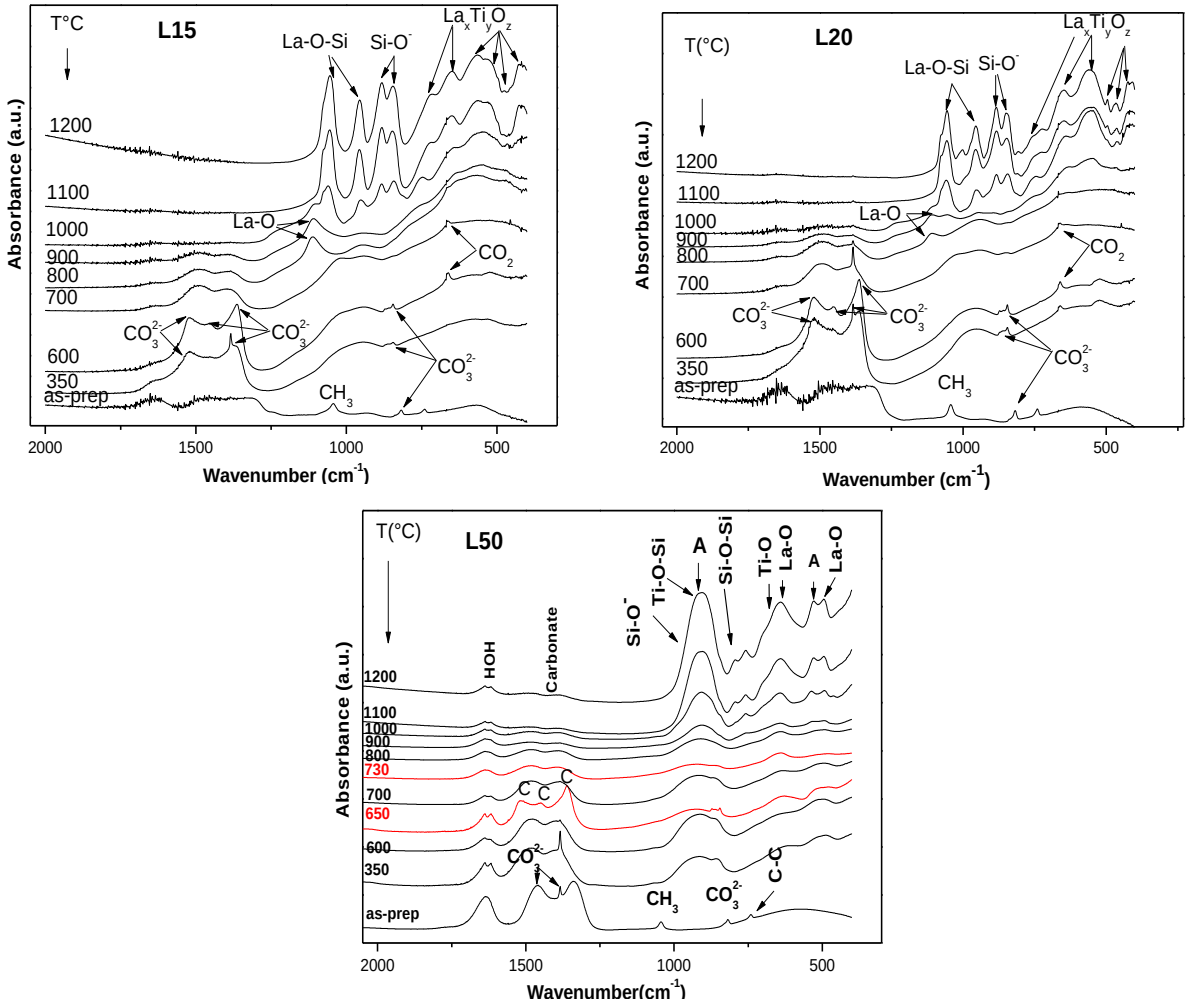

Figure 20. FTIR spectra of the L15, L20 and L50 microparticles.

The recorded FTIR spectra for L15, L20 and L50 samples are presented in the Figure 20 and the infrared absorption bands assignments in Table 6-8.

Table 6. Infrared absorption bands assignments of the as-prepared and 350, 600, 700°C L15 and L20 annealed samples.

T(°C)	Wavenumber (cm^{-1})			Band assignments	Phases
as-prepared	350°C	600°C	700°C		
1622				HOH band	
1455 ,1340	1523,1360	1523,1360,1460	1500,1364,2344	CO_3^{2-}	La_2CO_5
826	850	850		CO_3^{2-}, Si-O	La_2CO_5
	662	662	662	OCO	La_2CO_5
	518	518		CO_2^-	La_2CO_5

Table 7. Infrared absorption bands assignments of the 800, 900, 1000, and 1100°C L15 and L20 annealed samples.

T(°C)		Wavenumber (cm^{-1})		Band assignments	Phases
800°C	900°C	1000°C	1100°C		
475	1105,475	1105	1114	La-O	La_2O_3
		950-1065	950-1065	La-O-Si	
		842-884	842-884	$Si-O^-$	SiO_2
		760,650,556,492,466,420	760,650,556,492,466,420		$La_xTi_yO_z$

Table 8. Infrared absorption band assignments of the as-prepared and 350, 650 and 730°C L50 annealed sample.

T(°C)	Wavenumber (cm^{-1})			Band assignments	Phases
as-prepared	350°C	650°C	730°C		
1638	1638	1638	1631	HOH band	
1455 ,1340	1485,1386	1485,1378	1485,1378	CO_3^{2-}(1)	La_2CO_5
835	889	889	858	CO_3^{2-}(3)	La_2CO_5
			491, 639 cm^{-1}	La-O	La_2O_3

Table 9. Infrared absorption band assignments of the 800, 900, 1000 and 1100°C L50 annealed sample.

T(°C)		Wavenumber (cm^{-1})		Band assignment	Phases
800°C	900°C	1000°C	1100°C		
1634				H_2O	
913-521	913-521	913-532	913-524		$La_{9.33}Si_6O_{26}$
958	958	958	958	La-O-Si	
		852-983	852-983	$Si-O^-$	SiO_2

3.4 Raman

The Raman peaks observed at 240, 355, 758, and 840 cm^{-1} (Figures 21) are assigned to apatite phase $La_{9.33}Si_6O_{26}$, in good agreement with the Raman spectrum of apatite lanthanum silicate phase in reported by Rodriguez-Reyna et al [43]. As we can see these bands appear from 800°C heat treated sample and are increasing in intensity with calcinations temperatures, these results are a good correlation with XRD patterns.

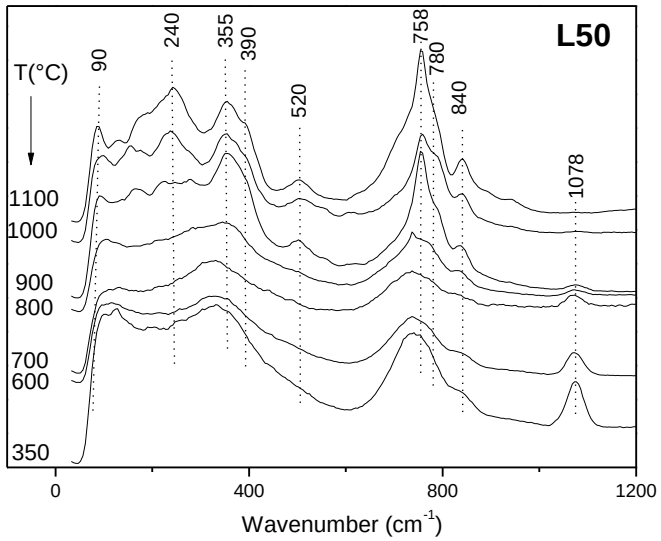

Figure 21. Raman spectra of the La50 sample.

Table 10. The main Raman spectral bands for L50 sample.

Raman wavenumber (cm^{-1})	**Band assignement**
1070	La_2CO_5
310, 355, 445	La_2O_3
240, 270, 355, 375, 840	$La_{9.33}Si_6O_{26}$
90, 780	La_2TiO_5
125, 206, 390, 510	SiO_2
935	Si-O-Ti
800	Si-O-Si
755	Si-O and O-Si-O
705	Ti-O-Ti
605	Si-O

The two characteristics band around 840 and 390 cm^{-1} can be assigned to the symmetric stretching mode of SiO_4 group [44]. The bands at 125, 206, 390, and 510 cm^{-1} indicate the presence of coesite SiO_2 phase, and the band around 520 cm^{-1} is associated with the asymmetric bending mode of SiO_4 tetrahedra and its grow with the calcinations temperature could be observed. It appears, therefore, that La ions have an ability to depolymerise the silica network, producing SiO_4 units that will be investigating in the apatite phase [45]. The Raman spectra show an intense band at 1070 cm^{-1} assigned to lanthanum carbonate [46,47] for the 350, 600 and 700°C treated samples. These results are good agreement with XRD results.

3.5 EPR

In the EPR spectra can be observed the same so called U-spectra characteristic for the Gd^{3+} ions, as we describe before for the samples with lower lanthanum concentration. For the microparticles heat treated at 1100°C and 1200°C one can see that the lanthanum prevents the formation of oxygen vacancies. According with XRD patterns of the microparticles with high lanthanum content a new crystallin phase are developing at high thermal treatment and the EPR spectra indicating the integration of Gd^{3+} ions in these phases. The ionic radii for Gd^{3+}, Ti^{4+}, Si^{4+} and La^{3+} are 0.93, 0.68, 0.5 and 1.06Å, respectively. The Gd^{3+} ions can easly substitute the Ti^{4+} place due to to their ionic radii which are very close in values. Therefore can be concluded that the Gd^{3+} ions are integrated in the $La_2Ti_2O_7$ phase for the both L15 and L20 systems heat treated at 1000°C. Considerring the ionic radii values for Gd^{3+} and La^{3+} can be assume that the Gd^{3+} ions are integrated for lanthanum containing heat treated samples in the unidentified phase which should be a lanthanum based phase $La_xTi_yO_z$ (Figure 22).

It is known that the fully decarbonated La_2O_3 can generate paramagnetic superoxide ion, detectable by EPR [48] around g ~ 2.000±0.001. It has been demonstrated also that in insulators materials at elevated temperature holes and electrons may be traped at certain oxide ions and by molecular oxigen, respectively, to form O^- and O_2^- centres [49]. The EPR spectra of O^{2-} on La_2O_3 is also known to have a paramagnetic signal at g ~ 2.006, but can increase by 0.003, the variation beeing reflected by the problem of removing carbonate impurities from the surface [50]. The EPR signals for the L15 and L20 systems heat treated from 700 to 1000°C and 700 to 1200°C, respectively (red spectra), can be discussed acoording with Xiang results. Should be also mentioned that in the XRD patterns for these samples can be evidenced the La_2O_3 phase.

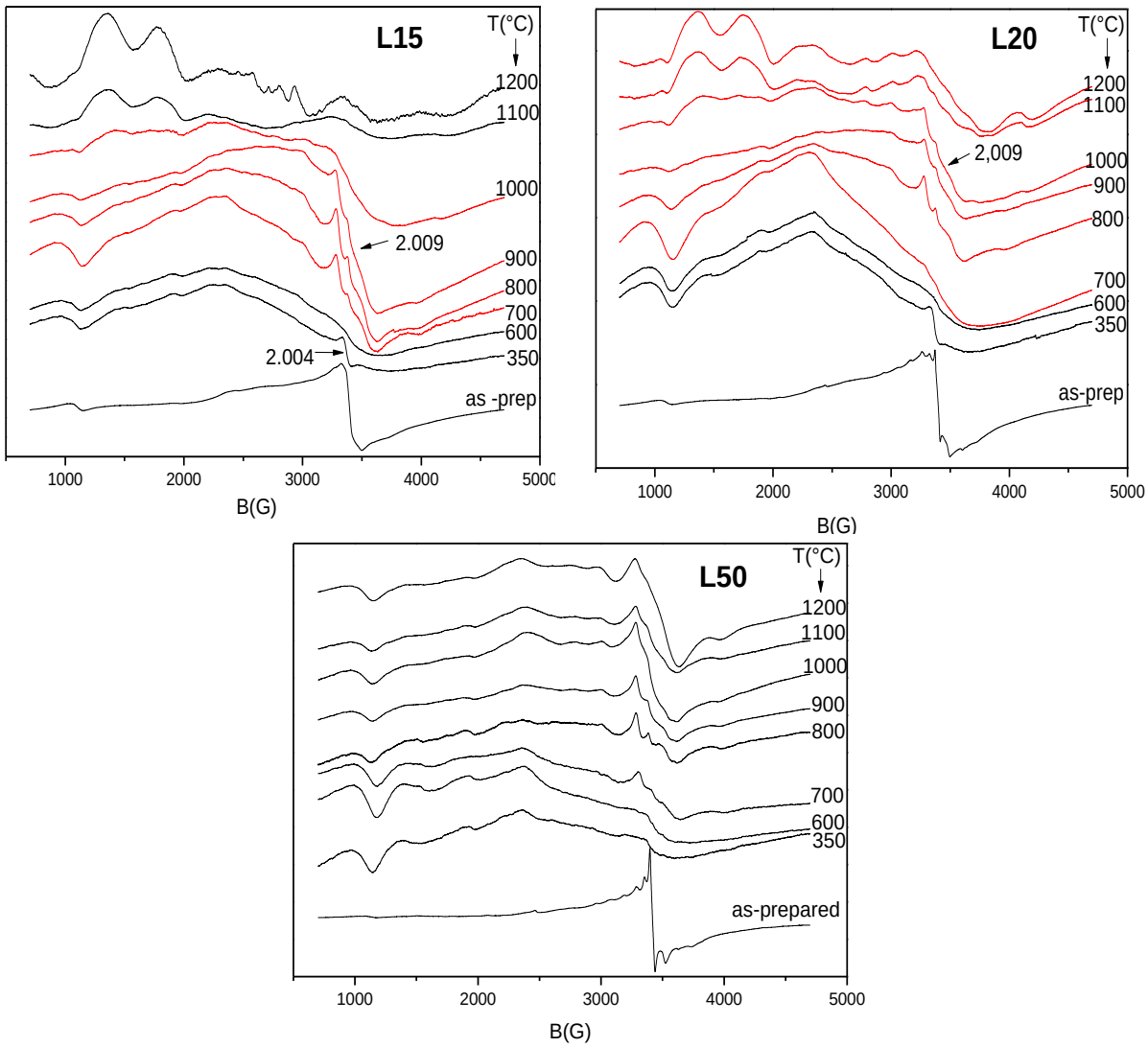

Figure 22. EPR spectra of the L50 microparticles.

The EPR results show (Figure 22) for the as-prepared and 350°C heat treated L50 sample the U-spectrum of Gd^{3+} with characteristic lines at g=5.9, g=4.8, g=2.85, g=2.0, after the 600°C the samples exhibits an EPR asymmetric signal characteristic of O_2^-. In the case of

La_2O_3 the value g_{zz}=2.063-2.093 have been reported by Loginov at al. This problem may reflect the problem of removing carbonate impurities from the surface [49]. The signal for 700°C heat treated sample exhibits a line shape with different g values (g_{zz}=2.044, g_{yy}=2.009, and g_{xx}=2.005) that are in good agreement with those obtained for O_2^- in La. For the L50 sample the Gd^{3+} ions are integrated in the apatite phase that is developing above 800°C.

3.6 NMR

There were registered the ^{29}Si MAS-NMR spectra for the L15 and L50 as-prepared microparticles and performed deconvolution with components having chemical shifts corresponding to different $Q^{(n)}$ units in order to estimate the distribution of silicate tetrahedra.

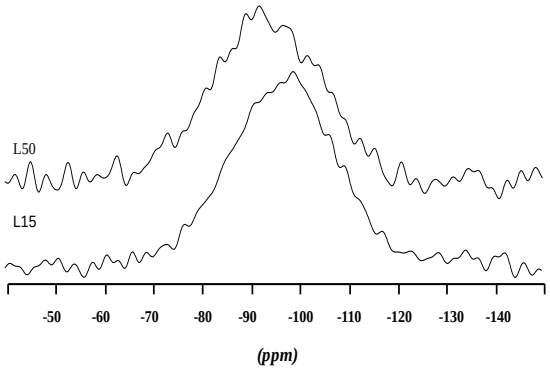

Figure 23. ^{29}Si NMR sperctra of L15 and L20 as-prepared samples

The 29Si MAS NMR spectra of the L 15 and L50 as prepared samples (Figure 23) indicate the presence of Q^4, Q^2, Q^1 and Q^0 units, presented also in the sample with lower lanthanum content. From the chemical shift, relative fraction (%) and the width of Q^n units, no significant differences can be observed between these samples. However, can be observed that in the L50 microparticles are slightly higher degree of disorder.

Table 11. Isotropic ^{29}Si chemical shift (A), relative fraction (%) (B) and width (C) of Q^n units data for the as-prepared L15, L50 microparticles.

Q^n (ppm) / X (% La)	Q^0	Q^1	Q^2	Q^4
15	-75.87	-86.33	-97.96	-110
50	-75.87	-85.5	-94.84	-109.34

Q^n (%) / X (% La)	Q^0	Q^1	Q^2	Q^4
15	3.53	16.87	63.28	16.32
50	1.75	17.23	78.3	2.73

Q^n (ppm) / X (% La)	Q^0	Q^1	Q^2	Q^4
15	7.51	12.54	19.06	21.36
50	13.81	18.1	23.28	9.31

3.7 XPS

The development of different crystalline phases on the material' surfaces have important application in the catalyse field. ***L15:*** From the relative percentage of the main components determined before and after the differents heat treatments (Table 11) can be observed that the lanthanum percentage increase on the miroparticles surface up to 350°C thermal treatment. For the 350°C thermal treatment one can see that only La, C and O atoms are presented on the microspheres surface and the atomic percentage for these elements are compared to the one calculated for La_2CO_5. By corelating this analysis with XRD results

where La_2CO_5 is the only crystalline phase developed at this temperature, one can conclude that the La_2CO_5 phase predominates on the samples surface. This result is very important for the catalyst application. The carbon concentration on the surface decreases due to the both residual carbonates from the precursors and La_2CO_5 decomposition into La_2O_3, according with XRD results.

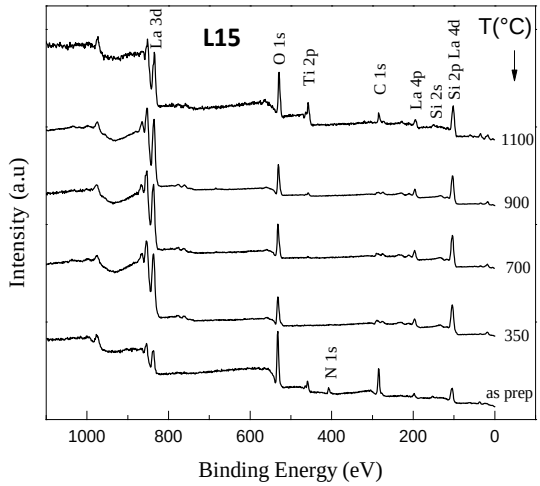

Figure 24. Survey spectra of the L15 microspheres.

Table 12. Relative percentage of the main elements for L15 sample determined before and after the different heat treatments

T(°C)	Elemental composition (%at)					
	O	C	La	Ti	Si	Ti/Si
as prep	42.82	50.98	2.59	3.61	-	-
350	63.2	20.4	16.4	-	-	-
700	62.43	21.33	15.8	0.44	-	-
900	63.9	14.19	19.42	2.49	-	-
1100	47.72	27.71	7.47	9.9	7.2	1.37

L50: Can be observed in the as prepared survey spectra the presence of N 1s. The Table 19 shows the percentage of the atomic concentrations of the main components for different heat treatments. The Pauling electronegativity value of Ti is 1.5 and of La is 1.1 [51,52]. In this case the possibility of electron transfer from lanthanum to titanium is favourable in Ti-O-La bridges.

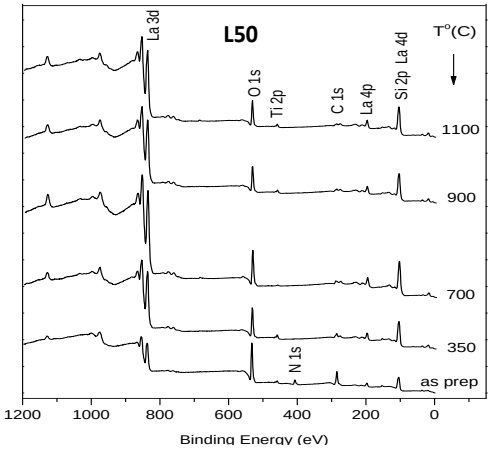

Figure 25. Survey spectra of the L50 microparticles.

Table 13. Relative percentage of the main components for L50 sample determined before and after the different heat treatments

T(°C)	O	C	La	Si	Ti	Ti/Si
as prep	50.7	38.8	4.9	4.3	1.3	0.3
350	53.64	22.05	15.68	5.43	3.2	0.59
700	62.99	14.69	21.71	-	0.61	-
900	58.18	13.55	21.33	4.10	2.84	0.69
1100	55.68	12.72	22.45	6.11	3.04	0 .49

CONCLUSIONS

There were synthesized by spray drying the hydrolysed and polycondensated titanosilicate sol, microparticles of less than 5 μm in diameter and specific nanocrystals were developed by thermal treatments. The pH was adjusted to a suitably low value to stabilize the sol by minimizing the rate of polycondensation, thereby allowing storage stability of the sol prior to spraying. The spray-dry method was successfully used for the chosen materials synthesis because of the flexibility to obtain multi-component oxide systems under a relatively low temperature. From manufacturing point of view, this method offers the advantage of being single-step process that can be readily scaled up. Using this technique the number of unit operations is reduced, improving production efficiency and reducing costs, especially since spray drying is a technique that can be easily automated and equipped for in-line product analysis.

The as-prepared microspheres were found to be non-crystalline confirmed by XRD patterns. The DTA curves distinguish the water loss and the organic component decomposition temperatures and also the temperature of the maximum crystallization process. By XRD patterns have been identified the crystalline phases (anatase, rutile, SiO_2, La_2O_3, $La_2Ti_2O_7$, La_2TiO_5, $La_4Ti_9O_{24}$ and $La_{9.33}Si_6O_{26}$ apatite phase) formed in polycrystalline microparticles obtained after heat treatments and it was also found that lanthanum content fosters the formation of nanocrystallites with smaller size. This decreasing of the crystallites size is an important phenomenon in catalysis process. The presence of $La_{9.33}Si_6O_{26}$ apatite phase in samples with high lanthanum content makes these materials suitable in fuel cells, oxygen sensors or separation membranes applications. For the 20% La_2O_3 and especially for 15%La_2O_3, the predominant phase developed was $La_2Ti_2O_7$, an intensively investigated phase in the literature for being a pyrochlore structure, potentially useful for a range of technological applications.

The samples were doped with gadolinium in order to extend the investigation of the samples by electron paramagnetic resonance spectroscopy, one of the most efficient methods for the characterisation of local order and magnetic interaction in crystalline and non-ctystalline systems. The changes in the local order around Gd^{3+} ions support the assumption

that Gd^{3+} ions are integrated in the nanocrystalline phases developed after heat treatment substituting lanthanum from these phase.

By increasing the La_2O_3 content in the titanosilicate matrix leads to high refractive index microparticles achieving. ^{29}Si MAS NMR measurements have been evidenced the segregation of the SiO_2 for the as prepared samples by increasing the lanthanum content. The sample with 1% La_2O_3 content seems to have the best amorphous character and a major achievement of this sample is the presence of anatase phase for this concentration until 1100°C heat treatment. The presence of anatase phase was identified by XRD analysis and confirmed by Raman measurements.

For the samples with low lanthanum content the XPS analyses point out that the thermally treated microspheres have surfaces rich in silica amount, while the titanium dominates inside. These results, completed by XRD patterns, SEM imagines and EDX analyses support the idea that the thermally treated microspheres surfaces are and remain covered by a silica layer in amorphous state. The thermal treated microspheres have a friendlier surface for future interaction with biological environments allowing them to integrate with the surrounding native tissue.

For a high La_2O_3 content (15-50%) La_2CO_5 crystalline phase is developed on the samples surface, a very important result for the catalytically application. The transition temperature from La_2CO_5 to La_2O_3 crystalline phase increases by lanthanum oxide addition to the matrix.

SELECTED BIBLIOGRAPHY:

[1] J. Yu, J. C. Yu and X. Zhao, J. Sol-Gel Sci. Tech. 24, (2002), 95.

[2] S. Hong, M. S. Lee, S. Park and G. Lee, Catal. Today 87, (2003), 99.

[3] A. Nilchi, S. Janitabar-Darzi, S. Rasouli-Garmarodi, Materials Sciences and Applications, (2011) 2, 476-480.

[4] Mohamed,I.A.Mkhalid, Journal of Alloys and Compounds,volume 501, pages 143-147 (2010).

[5] K.T. Ranjit, I. Willner, S.H. Bossmann, A.M. Braun, Lanthanide oxide-doped titanium dioxide photocatalysts: novel photocatalysts for the enhanced degradation of *p*-Chlorophenoxyacetic acid, Environ. Sci. Technol. 35 (2001)1544.

[6] Zhang, H.X. Zhang,Y.X.Xu,Y.G.Wang, Europium doped nanocrystalline titanium dioxide: preparation phase transformation and photocatalytic properties,J. Mater. Chem. 13 (2003) 2261.

[7] Gao; Wachs, I.E.Catal.Today 1999, 51, 223.

[8] Y. Zang, Y. Wu, M. Chen, L. Wu, Colloids and Surfaces A: Physicochem. Eng. Aspects 353 (2010) 216-225.

[9] W. Dong, C.W. Lee, X. Lu, Y. Sun, W. Hua, G. Zhuang, S. Zhang, J. Chen, H. Hou, D. Zhao, Appl. Catal. B-Environ. 95 (2010) 197-207.

[10] H. Nur, Mater. Sci. Eng., B 133, 1-3 (2006) 49-54

[11] M.S. Dadash, S. Karbasi, M.N. Esfahani, M.R. Ebrahimi, H. Vali, J. Mater. Sci. Mater. Med. 22 (2011) 829–838.

[12] Shibli, S. Mathai, J. Mater. Sci. Mater. Med. 19 (2008) 2971–2981.

[13] V. Ääritalo, S. Areva, M. Jokinen, M. Lindén, T. Peltola , J. Mater. Sci. Mater. Med. 18 (2007)1863-1873.

[14] Areva, V. Aäritalo, S. Tuusa, M. Jokinen, M. Lindén, T. Peltola, J. Mater. Sci. Mater. Med. 18 (2007) 1633–1642.

[15] A.M. Seco, M.C. Gonçalves, M.R. Almeida, Mater. Sci. Eng., B 76 (2000) 193–199.

[16] O. Ponta, E. Vanea, **A. Cheniti**, P. Berce, S. Simon,Materials Chemistry and Physics, Volume 135, Issues 2–3, 15 August 2012, Pages 863–869.

[17] Kapoor, J. Cell. Biochem. (2009) 106, 193.

[18] Feng, H. Xiao, X. He, Z. Li, F. Li, N. Liu, Y. Zhao, Y. Huang, Z. Zhang, Z. Chai, Toxicol. Lett. (2006) 165, 112.

[19] Fei, L. Yuanlei, W. Yang, X. An, L. Guohui, J. Rare Earths 25 (2007) 359.

[20] Bernard, L. Anthony, A. Daniel, R. Nadya, M. Natalie, B.D. Tilman, Kidney Int. (2005) 67, 1062.

[21] Paiva, M.S. de Oliveira, S.N. Yunes, L.G. de Oliveira, J.B. Cabral-Neto, C.E.B. de Almeida, Bull. Environ. Contam. Toxicol. (2009) 82, 423.

[22] Guan, Y.-S. Yin, Mater. Chem. Phys. (2005) 92, 10.

[23] Nalt. Bur. Stand. (U.S.) Monogr. 25, 7, 82 (1969).

[24] M.Todea, R.V.F.Turcu, B.Frentiu, M.Tamasan, H.Mocuta, O.Ponta, S.Simon, J. Mol. Struct. 1000 (2011) 62–68.

[25] O. Ponta, H. Mocuta, M. Vasilescu, S.Simon, J Sol-Gel Sci Technol, 58 (2) (2011) 530-534.

[26] S. Simion, A.D. Udvar, J. Am. Ceram. Soc. 93, 2760 (2010) 1-4.

[27] S. Simon, R. Pop, V. Simon, M. Coldea, J. Non-Cryst. Solids, 331, 1 (2003).

[28] E.Culea, L.Pop, S. Simon, Mater. Sci. Eng. B 112:59 (2004).

[29] Hussain, Y. Prabhakara Reddy, S. Buddhudu, Mater. Res. Bull. 36 (2001) 1813.

[30] Kliava, A. Malakhovskii, I. Edelman, A. Potseluyko, E.A. Petrakovskaja, S. Melnikova, T. Zarubina, G. Petrovskii, Y. Bruckental, Y. Yeshurun, Phys. Rev. B 71 (2005) 104406.

[32] Li, D.S. Hwang, N.H. Lee, S.J. Kim, Chem. Phys. Lett. 404 (2005) 25–29.

[33] Fittipaldi, V. Gombac, T. Montini, P. Fornasiero, M. Graziani, Inorg. Chim. Acta 361 (2008) 3980–3987.

[34] Feng, Y. Wang, Z. Jin, J. Zhang, S. Zhang, Z. Wu, Z. Zhang, New J. Chem. 32 (2008) 1038–1046.

[35] Kuznetsov, N. Serpone, J. Phys. Chem. C 113 (2009) 15110–15123.

[36] Zhang, P. J. Grandinetti, J. F. Stebbins, J. Phys. Chem. B 101 (1997) 4004.

[37] Massiot, F. Fayon, M. Kapron, I. King, S. Le Calve, B. Alonso, J.-O. Durand, B. Bujoli, Z. Gan, G. Hoatson, Magn. Reson. Chem. 40 (2002) 70.

[38] Sheng ,CAI Wei-ping, WAN Li-xi, SHI Ming-da, LUO Xiang-dong, JING Wei-ping Trans nonferrous Met. Soc. China 19(2009) s743-s747.

[39]Carlos Vazquez-Vasques, M.Arturo Lopez-Quintela, Journal of solid state Chemistry 179(2006) 3229-3237.

[40] Célérier, C. Lberty, F Asart, P. Lenormand, P. Stevens, Ceram. Int. 32(2006) 271.

[41] Nakayama, M. Higuchi, J. Mater.Sci.Lett.2001, 20, 913.

[42] **A. Cheniti**, O.Ponta, L.Tarle, T. Radu, S. Simon, Optoelectronics and Advanced Materials – Rapid Communications Vol. 6, No. 5-6, May - June 2012, p. 560 – 563

[43] Reyna, A. F. Fyents, M. Mczka, J. Hanuza, K. Boulahya, U. Amador, J. Solid State Chem.197 (2006) 522.

[44] Lucazeau, N. Sergent, T. Pagnier, A, Shaula, V. Kharton, F.M.B. Marques, J. Raman Spectrosc. 38 (2007) 21.

[45] Kepinski, Woldzimierz Mista, Janina Okal, Marek Drozd, Miroslaw Maczka, Silid State Sciences 7 (2005) 1300-1311.

[46] Vieira,J.C Oliveira, A.L.Shaula, A.Cavaleiro, B.Trindade; Surafce Coatings Technology 206 (2012) 3316-3322.

[47] Klingenberg, M. A. Vannice, Chem. Mater.8 (1996) 2755.

[48] Louis, Tien Lin Chang,Maggy Kermace,Tiep Le Van Jean Michel Tatibouet and Lichel che; Catalysis Today, 13 (1992) 283-289

[49] Wang and Jack H. Lunsford, J. Phys. Chem. 1986, 90, 3890-3891.

[50] Xiang, Jack H. Lunsford; J.Phys. Chem. 1986, 90, 3890-3891.

[51] Benjaram Reddy,Biswajit Chowdhury, Panagiotis G. Smirniotis, Applied Catalysis A: Generall.Volume 219(2001) 53-60.

[52] Lee, Concise Inorganic Chemistry, 4th Edition, p. 160.